Available online at www.sciencedirect.com
SCIENCE DIRECT®
Journal of Power Sources 129 (2004) 358–367
JOURNAL OF POWER SOURCES
www.elsevier.com/locate/jpowsour

Effect of the La/Mg ratio on the structure and electrochemical properties of $La_xMg_{3-x}Ni_9$ ($x = 1.6$–2.2) hydrogen storage electrode alloys for nickel–metal hydride batteries

B. Liao [a], Y.Q. Lei [a,*], L.X. Chen [a], G.L. Lu [b], H.G. Pan [a], Q.D. Wang [a]

[a] *Department of Materials Science and Engineering, Zhejiang University, Hangzhou 310027, PR China*
[b] *Central Laboratory, Zhejiang University, Hangzhou 310027, PR China*

Received 24 September 2003; received in revised form 5 November 2003; accepted 21 November 2003

Abstract

Effect of La/Mg ratio on the structure and electrochemical properties of $La_xMg_{3-x}Ni_9$ ($x = 1.6$–2.2) ternary alloys was investigated. All alloys are consisted of a main phase with hexagonal $PuNi_3$-type structure and a few impurity phases (mainly $LaNi_5$ and $MgNi_2$). The increase of La/Mg ratio in the alloys leads to an increase in both the cell volume and the hydride stability. The discharge capacity of the alloys at 100 mA/g increases with the increase of La/Mg ratio and passes though a maximum of 397.5 mAh/g at $x = 2.0$. As the La/Mg ratio increases, the high-rate dischargeability of the alloy electrodes at 1200 mA/g HRD_{1200} decreases from 66.7% ($x = 1.6$) to 26.5% ($x = 2.2$). The slower decrease of HRD_{1200} (from 66.7 to 52.7%) of the alloys with $x = 1.6$–2.0 is mainly attributed to the decrease of electrocatalytic activity of the alloys for charge-transfer reaction, the more rapid decrease of HRD_{1200} of the alloys with $x > 2.0$ is mainly attributed to the lowering of the hydrogen diffusion rate in the bulk of alloy. The cycling capacity degradation of the alloys is rather fast for practical application due to the corrosion of La and Mg and the large V_H in the hydride phase.

Keywords: Hydrogen storage alloy; Ni/MH battery; $PuNi_3$-type structure; Electrochemical property; Exchange current density; Hydrogen diffusion rate

1. Introduction

In recent years, nickel–metal hydride (Ni/MH) secondary batteries have been widely adopted in various portable electronic devices, electric hand tools and electric vehicles because of their good electrochemical performance and environment compatibility. To date, almost all commercial Ni/MH batteries are employing AB_5-type alloys as negative electrode materials due to their good overall electrode properties [1]. However, due to the limited electrochemical capacity (300–320 mAh/g) of the AB_5-type alloys, the energy density of the Ni/MH batteries are not competing favorably with some other advanced secondary batteries. Recently, a large number of research and development on higher energy density MH electrode alloys such as AB_2-type Laves phase alloys [2,3], Mg–Ni based amorphous alloys [4,5] and V–Ti–Ni based solid solution alloys [6] have been reported. However, these alloys are still suffering from slow activation, fast passivation and/or high rate of cycling degradation [7].

Recently, Kadir et al. [8–10] reported the discovery of a new type of ternary alloys with the general formula of RMg_2Ni_9 (R: rare earth, Ca, Y) and $PuNi_3$ type structure. It was found that some of the R–Mg–Ni based quaternary alloys could absorb–desorb 1.8–1.87 wt.% H_2 and were thus regarded as promising candidates for reversible gaseous hydrogen storage [11,12]. As to their electrochemical hydrogen storage, Chen et al. [13] reported that the discharge capacity of $LaCaMgNi_9$ alloy reached 356 mAh/g, and almost at the same time, Kohno et al. [14] reported that the discharge capacity of $La_{0.7}Mg_{0.3}Ni_{2.8}Co_{0.5}$ alloy reached 410 mAh/g, with fairly good cycling stability within 30 cycles. Furthermore, Pan et al. [15] studied the structure and electrochemical properties of $La_{0.7}Mg_{0.3}(Ni_{0.85}Co_{0.15})_x$ ($x = 2.5$–5.0) alloys, and found that the alloy with $x = 3.5$ had a maximum discharge capacity of 395.6 mAh/g, but its cycling stability was inferior to that reported by Kohno et al. [14]. In view of their higher electrochemical capacity, the La–Mg–Ni based alloys have been considered as the new candidates of the negative electrode materials of Ni/MH batteries for further investigation. However, up to now only very few studies have

* Corresponding author. Tel.: +86-571-8795-1152; fax: +86-571-8795-1152.
E-mail address: leiyq@sun.zju.edu.cn (Y.Q. Lei).

0378-7753/$ – see front matter © 2003 Elsevier B.V. All rights reserved.
doi:10.1016/j.jpowsour.2003.11.044

been devoted to the evaluation of the electrochemical properties of La–Mg–Ni system ternary alloys to provide useful information for the further development of this new group of alloys. In a previous paper [16], we indicated that the dimension of lattice parameters and the electrode properties of $La_xMg_{3-x}Ni_9$ ($x = 1.0, 1.2, 1.4, 1.6, 1.8, 2.0$) alloys were noticeably influenced by the La/Mg ratio in the alloys, but the study on alloy composition was not systematic enough and the kinetic properties of the alloy electrodes were neglected. In this work, we have reexamined the structure and electrochemical properties of the $La_xMg_{3-x}Ni_9$ ($x = 1.6$, 1.7, 1.8, 1.9, 2.0, 2.1, 2.2) alloys. The optimum amount of Mg substitution with La, the crystallographic structure, the electrochemical and kinetic behaviors of these alloy with different La/Mg ratios have been systematically studied.

2. Experimental

$La_xMg_{3-x}Ni_9$ ($x = 1.6$–2.2) alloy samples were prepared by sintering the mixtures of $LaNi_3$, $MgNi_2$ and Ni powders in different proportions as described in a previous paper [16]. These samples were mechanically pulverized to 300 mesh. Crystallographic characterization of the alloys was carried out with XRD analysis on a Rigaku RINT 2550/PC X-ray diffractometer with Cu Kα radiation at room temperature. These analyses were also made for the hydride samples of alloys under investigation. To avoid the desorption of hydrogen during the measurement, the electrochemically hydrided samples were coated with a glue as described by Chen et al. [13]. Pellet type alloy electrodes ($d = 10$ mm) were prepared by cold pressing the mixtures of different alloy powders and carbonyl nickel powder in the weight ratio of 1:3. Each alloy pellet was then interposed between two Ni foamed plates, the outer rims of which were then tightly spot-welded to keep a good contact between the pellet and Ni foamed plates. Electrochemical measurements were conducted at 25 °C in a conventional three-compartments electrochemical cell consisting of a working electrode (MH electrode), a Hg/HgO reference electrode, and a $NiOOH/Ni(OH)_2$ counter electrode, and the electrolyte of the cell was the 6 M KOH solution. The discharge capacity was determined galvanostatically by using an automatic charge–discharge unit. Each electrode was charged at 300 mA/g for 2 h followed by a 10 min rest, and then discharged at 100 mA/g to the cut-off potential of −0.6 V versus Hg/HgO. In evaluating the rate capability, discharge capacities of the alloy electrode at different discharge current densities were measured. The high rate dischargeability HRD (%) defined as $C_n \times 100/(C_n + C_{50})$, was determined from the ratio of the discharge capacity C_n (with $n = 400$, 800, 1200 mA/g, respectively) to the total discharge capacity defined as the sum of C_n and C_{50}, which was the additional capacity measured subsequently at 50 mA/g after C_n was measured. The electrochemical potential composition (EC) isotherms were plotted by using the pulse charge–discharge method at 25 mA/g, and the equilibrium hydrogen pressure P_{eq} was calculated from the measured equilibrium electrode potential E_{eq} according to the Nernst equation [17]:

$$E_{eq}(\text{V versus Hg/HgO}) = -0.9305 - 0.029547\log(P_{eq}), \qquad 25\,^{\circ}\text{C} \tag{1}$$

For investigating the electrocatalytic activity of the hydrogen electrode reaction, the linear polarization curves of the electrode were plotted with a Solartron SI 1287 potentiostat by scanning the electrode potential at the rate of 0.1 mV/s from −5 to 5 mV (versus open circuit potential) at 50% depth of discharge (DOD). The exchange current density (I_0), which is a measure of the catalytic activity of electrode, was calculated from the slopes of polarization curves by the following equation [18],

$$I_0 = \left(\frac{RT}{F}\right)\left(\frac{I}{\eta}\right)_{\eta\to 0} \tag{2}$$

where R is the gas constant, T the absolute temperature, F the Faraday constant, η the over-potential and I the applied current. The potentiostatic discharge technique was used to evaluate the coefficient of diffusion within the bulk of the alloy electrodes. After being fully charged followed by a 30 min open-circuit lay-aside, the test electrodes were discharged with +300 mV potential-step for 3000 s on a Solartron SI1287 potentiostat, using the CorrWare electrochemical/corrosion software.

3. Results and discussion

3.1. Crystal structure

From XRD analysis and metallographic examination, it is found that all the sintered samples contain a main phase and a few impurity phases including $LaNi_5$ and $MgNi_2$, which were probably resulted from incomplete sintering. The crystal structures have been identified and refined by means of X-ray powder diffraction data. For all samples, the main phase can be identified as the hexagonal $PuNi_3$ type structure belonging to the R-3m space group ($Z = 3$). Fig. 1 shows the typical XRD pattern of the La_2MgNi_9 alloy, and the final Rietveld structural parameters are tabulated in Table 1. The crystallographic results reveal that La atoms in La_2MgNi_9 are located not only at the 3a site (the Pu1 atom position of $PuNi_3$ structure), but also at the 6c sites (the Pu2 atom position of $PuNi_3$ structure), while Mg atoms in the alloy exhibit a strong preference for the 6c site, indicating that the alloy is a ordered ternary compound with the same structure as the previously reported RMg_2Ni_9 (R: La, Ca, Y) alloys [8–10,12].

Fig. 2 shows the relation of lattice parameters and unit cell volume of the $La_xMg_{3-x}Ni_9$ alloys with x ($x = 1.6$–2.2). It can be seen that the increasing of La content causes a linear increase in lattice parameters and the cell volume.

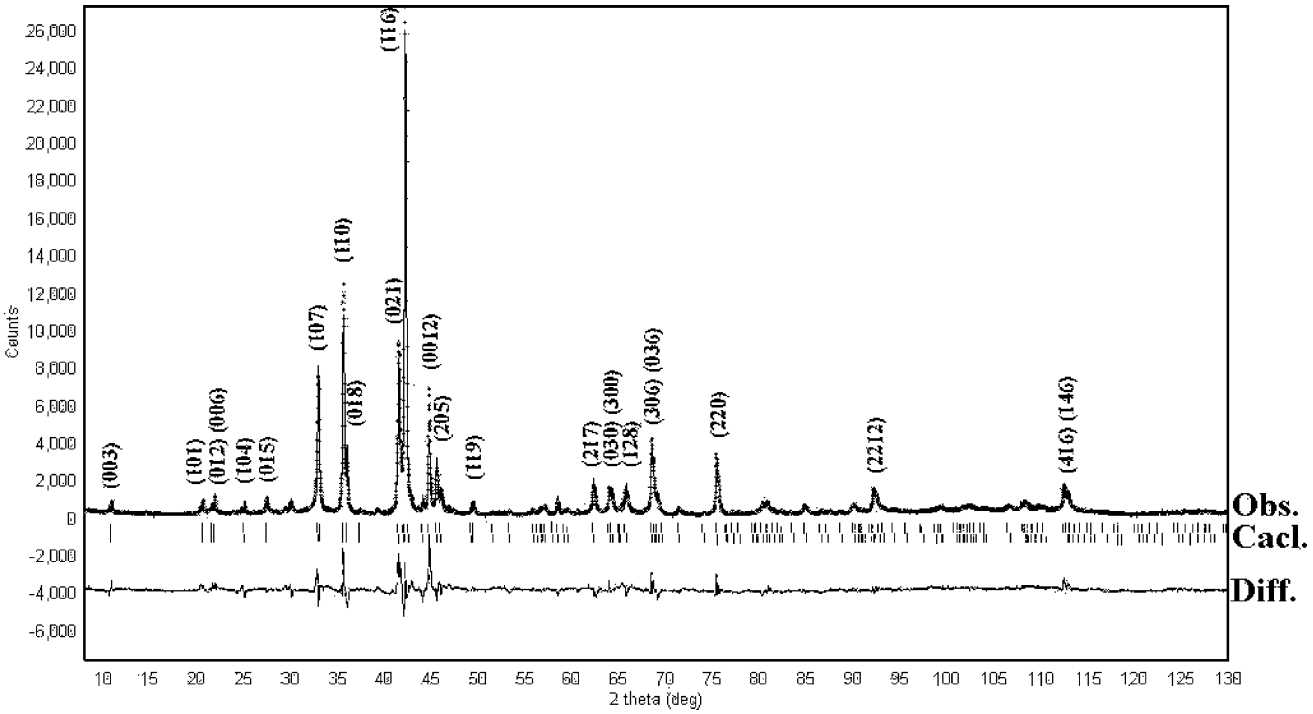

Fig. 1. Rietveld profile refinement of XRD patterns of La_2MgNi_9 alloy.

It is found that the progressive substitution of Mg by La in the alloys (from $x = 1.6$–2.2) leads to an increase of both *a* parameter (+0.87%) and *c* parameter (+1.09%) and a subsequent expansion of the unit cell volume (+2.87%) owing to the larger atomic radius of La (2.74 Å) than that of Mg (1.72 Å). Besides, the value of *c*/*a* remains almost constant, around 4.82–4.83 when the unit cell volume (Å^3) expands from 523.1 ($x = 1.6$) to 538.1 ($x = 2.2$). It means that the structure of these alloys is kept isotropic during expansion.

From the XRD analysis performed for the electrochemically hydrided $La_xMg_{3-x}Ni_9$ ($x = 1.6$–2.2) samples, it is also found that all the hydrided alloys still preserve the hexagonal $PuNi_3$-type structure, which was also observed in some RMg_2Ni_9 type alloys [9–11], but has a noticeably cell volume expansion due to hydriding. The data on the volume expansion rate of the unit cell during hydriding, $\Delta V/V$ and the molar volume of hydrogen, V_H, in the hydride phases are listed in Table 2. V_H is defined as the volume expansion of the unit cell per H atom absorbed and was calculated via $V_H = \Delta V/n$, where *n* is the number of H atoms charged into the unit cell and subsequently discharged [7]. It can be seen that the increasing of La content in the alloys (from $x = 1.6$–2.2) leads to an increase of both $\Delta V/V$ (from 19.5 to 25.9%) and V_H (from 3.27 to 3.77 Å^3 per H atom). This result reveals that the values of $\Delta V/V$ and V_H of the La–Mg–Ni system ternary alloys with $PuNi_3$-type structure are close to $LaCaMgNi_9$ quaternary alloy with the same structure ($\Delta V/V = 26.3\%$, $V_H = 3.44$) as observed by Chen et al. [12,13]. It is interesting to note that they are much larger than that of the commercialized $MmNi_{3.55}Co_{0.75}Mn_{0.4}Al_{0.3}$ electrode alloy ($\Delta V/V = 14.3\%$, $V_H = 3.23$) with $CaCu_5$-type structure as reported by Reilly [7].

Table 1
Crystallographic parameters for La_2MgNi_9 in a space group *R*-3*m* ($Z = 3$)

Atom	Site	Metal atom position			Occupy
		x	*y*	*z*	
La1	3a	0	0	0	1
La2	6c	0	0	0.14753 (13)	0.485
Mg1	6c	0	0	0.14753 (13)	0.515
Ni1	6c	0	0	0.32581 (23)	1
Ni2	3b	0	0	0.5	1
Ni3	18h	0.4941 (4)	0.5059 (4)	0.08276 (15)	1

The Rietveld refinement program Rietica was used.

3.2. Thermodynamic characteristics

The electrochemical pressure-composition isotherms measured at 25 °C for hydrogen desorption in the $La_xMg_{3-x}Ni_9$–H system are shown in Fig. 3. It can be seen that the desorption plateau pressure reduces noticeably as the La/Mg ratio of the alloys increases, decreasing from 0.379 atm for the alloy of $x = 1.6$ to a much lower value of 0.042 atm for the alloy of $x = 2.2$. This means that the hydrides of La-rich alloys are more stable than the hydrides of La-poor alloys because of the larger unit cell volume of the alloy with increasing La/Mg ratio. Fig. 4 shows the relationship between the unit cell volumes of $La_xMg_{3-x}Ni_9$ ($x = 1.6$–2.2)

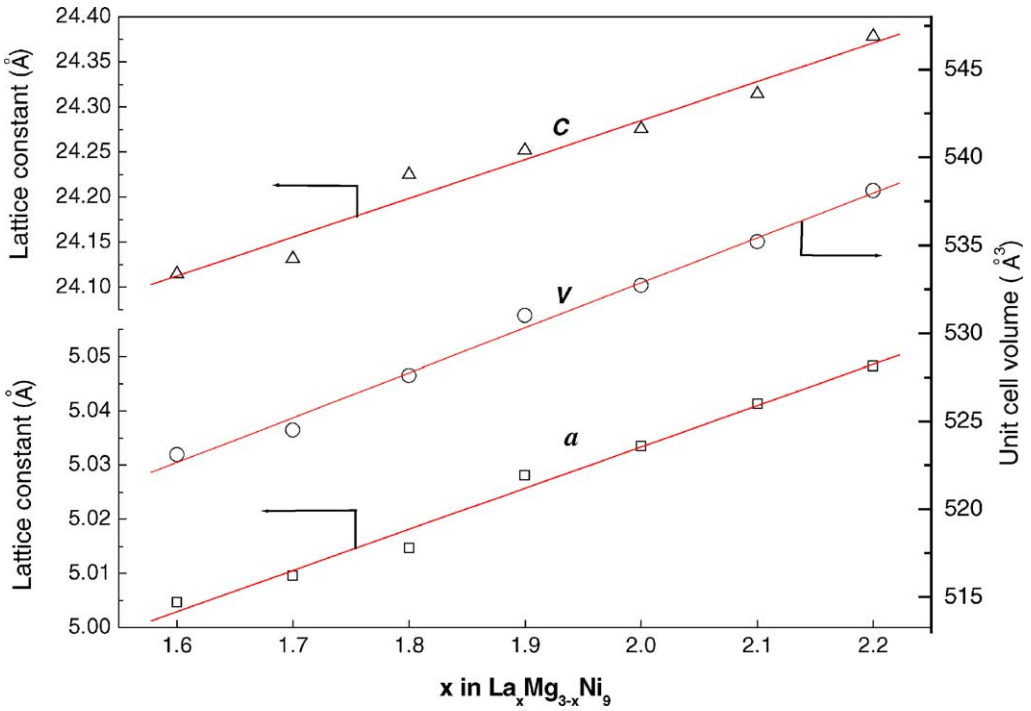

Fig. 2. Variations of the cell parameters and volume as the function of x in $La_xMg_{3-x}Ni$ alloys ($x = 1.6$–2.2).

alloys and the plateau pressures of their hydrides at 25 °C. A linear correlation between $\log P_{plateau}$ and the cell unit volume is observed for these alloys. The linear degradation of the logarithm of plateau pressure with increasing cell unit volume observed here is consistent with those reported previously for AB_3 alloys [12] and most AB_5 alloys [7].

As also shown in Fig. 3 and Table 2, the hydrogen storage capacity (H/M) increases from 0.751 to 1.03 when the La content increases from $x = 1.6$ to 2.0. However, as x increases further, the H/M decreases to 0.932 when x reaching 2.2. It is generally accepted that hydrogen storage alloys with larger unit cell volumes would result in more sites available for hydrogen storage. For the present alloys, the rule is obeyed in the composition range of $x = 1.6$–2.0. In the case of the alloys with composition of $x = 2.1$–2.2, the H/M value becomes lower than that for the alloy of $x = 2.0$ in spite of the increased unit cell volume. This is believed attributable to the high stability of the hydrides of the alloy with x beyond 2.0, too stable to desorb hydrogen readily during testing.

3.3. Charge–discharge characteristics

The activation property and maximum discharge capacity of the $La_xMg_{3-x}Ni_9$ ($x = 1.6$–2.2) alloy electrodes are listed in Table 2. It can be seen that all these alloys can be easily activated to reach the maximum capacity within three cycles. For the alloys with composition range of $x = 1.6$–2.2, the maximum discharge capacity C_{max} improves significantly with the increase in x and reaches a maximum at $x = 2.0$, and then decreases as x increases further. The variation of maximum discharge capacity of the alloys is basically consistent with the variation of the H/M with the La/Mg ratio in the alloys. The La_2MgNi_9 alloy shows a maximum dis-

Table 2
Summary of the electrode performances of $La_xMg_{3-x}Ni_9$ alloys ($x = 1.6$–2.2)

Alloys	H/M	C_{max} (mAh/g)	N_a[a]	HRD_{1200}[b] (%)	S_{100} (%)	$\Delta V/V$ (%)	V_H (Å^3 per H atom)
1.6	0.751	309.5	3	66.7	63.2	19.5	3.27
1.7	0.869	348.5	3	62.3	63.6	23.6	3.43
1.8	0.921	381.7	2	53.2	61.9	23.3	3.41
1.9	0.993	393.8	2	56.7	62.9	24.3	3.49
2.0	1.030	397.5	2	52.7	60.6	24.8	3.69
2.1	1.015	384.7	2	35.2	60.4	25.3	3.71
2.2	0.932	349.1	2	26.5	55.7	25.9	3.77

[a] The cycle numbers needed to activate the electrodes.
[b] The high rate dischargeability at the discharge current density of 1200 mA/g.

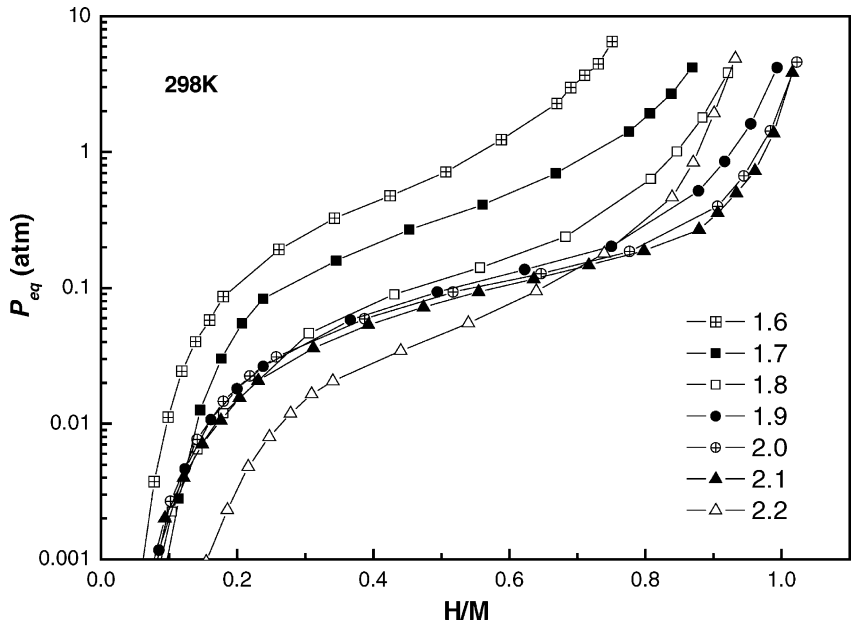

Fig. 3. The electrochemical desorption *P–C* isotherms for $La_xMg_{3-x}Ni_9$ alloys ($x = 1.6$–2.2) at 25 °C.

charge capacity of 397.5 mAh/g, which is noticeably higher than that of the commercialized AB_5-type alloys.

Fig. 5 shows the discharge curves (fourth cycle) of the $La_xMg_{3-x}Ni_9$ ($x = 1.6$–2.2) alloy electrodes at 100 mA/g and 25 °C. Obviously, each curve has a wide discharge potential plateau based on the oxidation of desorbed hydrogen from the hydride. Besides, the discharge plateau shifts toward a more positive potential as La content increases in the alloys. As shown in Fig. 5, the mid-discharge potential decreases from −0.8859 to −0.8464 V when *x* increases from 1.6 to 2.2, in agreement with the reduction of desorption plateau pressure with increasing La/Mg ratio in the alloys.

3.4. High-rate dischargeability and electrochemical kinetics

The HRDs of the alloy electrodes for the discharge current density of 1200 mA/g are also listed in Table 2. It can be seen that as the La content increases, the HRD_{1200} of the alloy electrodes decreases from 66.7% ($x = 1.6$) to 52.7%

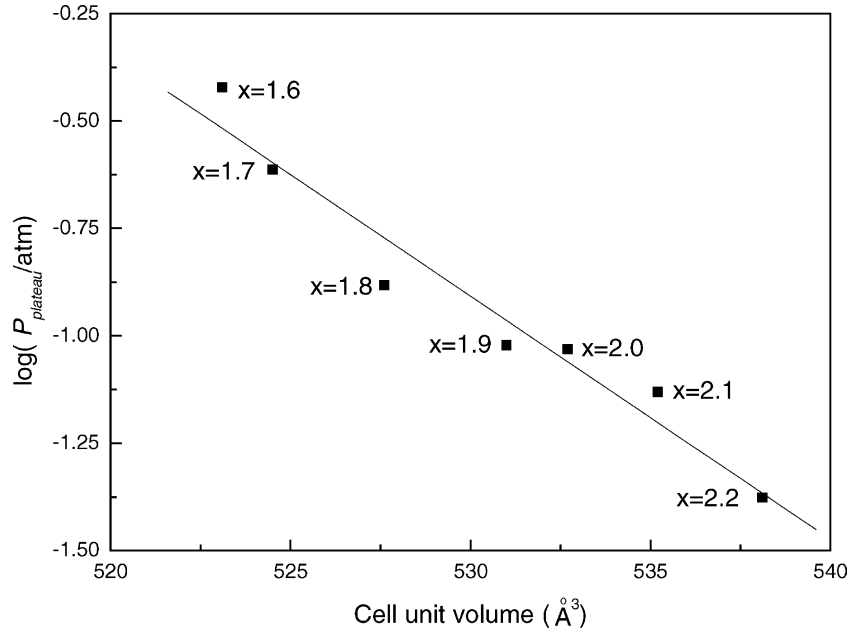

Fig. 4. Variation of the desorption pressure as a function of the cell volume of $La_xMg_{3-x}Ni_9$ alloys ($x = 1.6$–2.2).

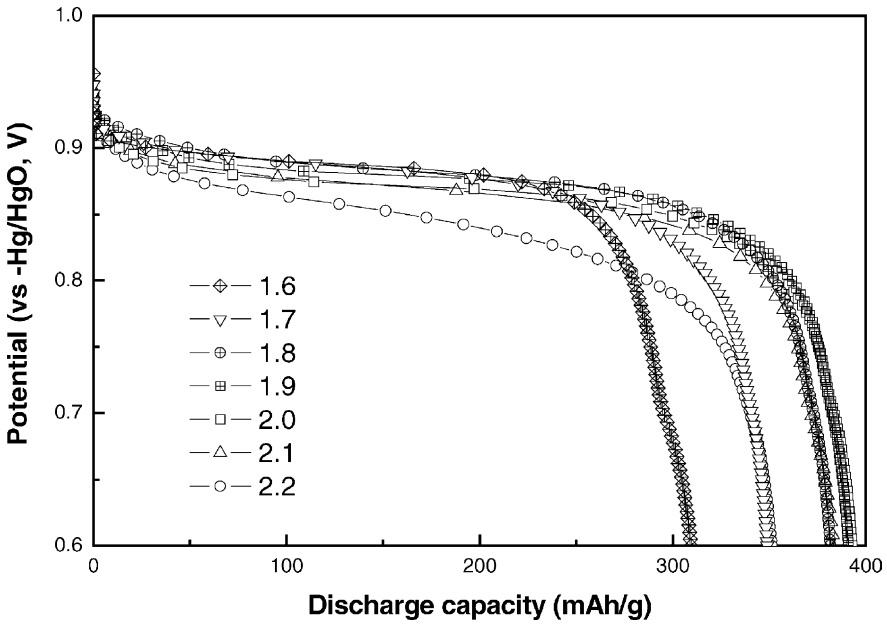

Fig. 5. The discharge potential curves of $La_xMg_{3-x}Ni_9$ alloys ($x = 1.6$–2.2) at discharge density of 100 mA/g (25 °C).

($x = 2.0$) except for the $La_{1.8}Mg_{1.2}Ni_9$ alloy electrode, the HRD_{1200} of which is lower than that of $La_{1.9}Mg_{1.1}Ni_9$. As the La content increases further, the HRD_{1200} decreases sharply to 26.5% at $x = 2.2$. It is known that the high-rate dischargeability of a metal-hydride electrode is mainly determined by the charge-transfer process occurring at the metal electrolyte interface and the hydrogen diffusion process in the hydride bulk [19,20]. From the linear polarization curves of the $La_xMg_{3-x}Ni_9$ alloy electrodes, the polarization resistance R_p and exchange current density I_0 of the alloy electrodes are calculated and shown in Fig. 6 as a function of x value. It can be seen that the polarization resistance R_p of the alloy electrodes increases with increasing x. Accordingly, the exchange current density I_0 of the alloy electrodes decreases from 135.4 to 69.5 mA/g when x increases from 1.6 to 2.2. Now let us look at the variation of I_0 value with the high-rate dischargeability (HRD_{1200}) of the alloy electrode as shown in Fig. 7. The high-rate dischargeability shows a linear relationship with the exchange density I_0 for the alloy electrodes with $x = 1.6$–2.0, suggesting that

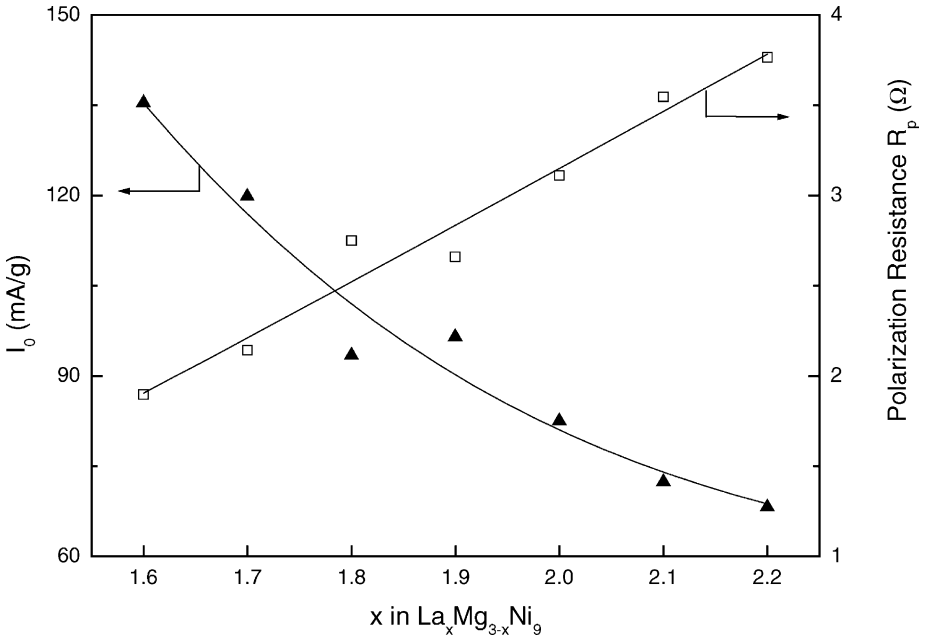

Fig. 6. The polarization resistance and the exchange current density of $La_xMg_{3-x}Ni_9$ alloy ($x = 1.6$–2.2) electrodes as a function of La content.

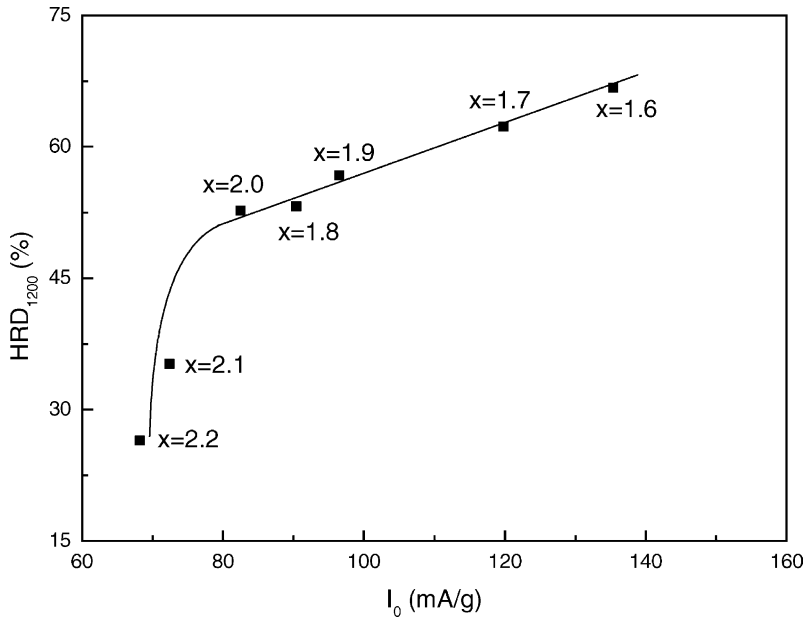

Fig. 7. High-rate dischargeability (HRD) at 1200 mA/g as a function of exchange current density (I_0).

the high-rate dischargeability of the alloy electrodes is essentially controlled by the charge-transfer reaction of the hydrogen at the discharge rate of 1200 mA/g. But the linear relationship no longer holds for $x = 2.1$–2.2 with the curve bending downwards sharply. It implies another factor, namely the hydrogen diffusion in alloy probably becomes the rate-determining factor for high-rate dischargeability.

The diffusion coefficient of hydrogen in the bulk of the alloys was determined by means of the potential-step method. Fig. 8 shows the semi-logarithmic plots of the anodic current versus time responses of the $La_xMg_{3-x}Ni_9$ ($x = 1.6$–2.2) alloy electrodes from the test. It can be seen that the current–time responses can be divided into two time domains [21], in the first time region, the oxidation current of hydrogen rapidly declines due to the rapid consumption of hydrogen on the surface. However, in the second time region followed, the current declines more slowly and drops linearly with time. Since hydrogen is supplied from the bulk of the alloy at a rate proportional to the concentration gradient of hydrogen, hence the electrode current is controlled by the diffusion of hydrogen in the second time region. Zheng et al. [21] reported that in a large anodic potential-step test,

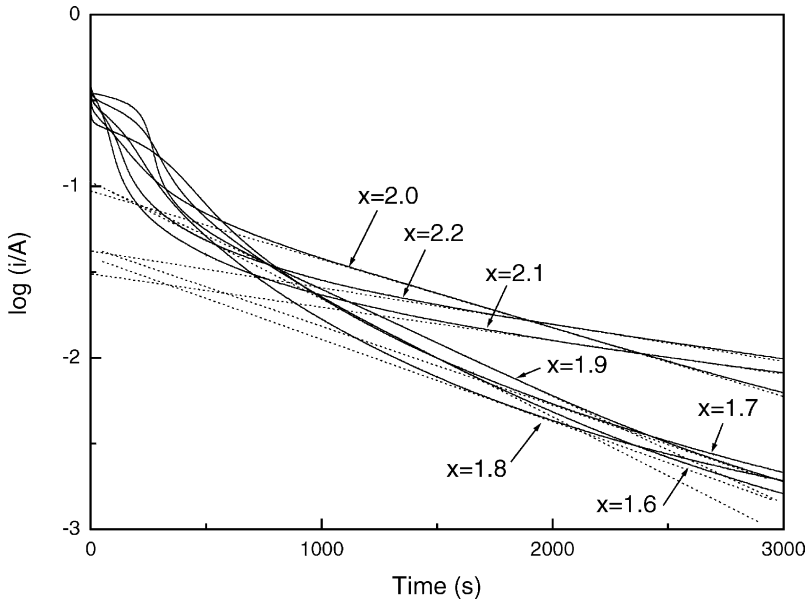

Fig. 8. Anodic current–time responses for $La_xMg_{3-x}Ni_9$ ($x = 1.6$–2.2) alloys electrodes after +300 mV potential-step.

Table 3
The ratio of D/a^2 and the hydrogen diffusion coefficient in the bulk of $La_xMg_{3-x}Ni_9$ alloys

Alloys	D/a^2 ($\times 10^{-4}$ s^{-1})	D ($\times 10^{-10}$ cm^2 s^{-1})
1.6	5.34	9.03
1.7	5.15	8.71
1.8	4.75	8.03
1.9	4.93	8.33
2.0	4.2	7.10
2.1	1.88	3.17
2.2	1.42	2.40

after a long discharge time, the diffusion current varies with time according to the following equation:

$$\log i = \log\left(\frac{6FD(C_0 - C_s)}{da^2}\right) - \left(\frac{\pi^2}{2.303}\right)\left(\frac{D}{a^2}\right)t \qquad (3)$$

where D is the hydrogen diffusion coefficient (cm^2/s), a the radius of the spherical particle (cm), i the diffusion current density (A/g), C_0 the initial hydrogen concentration in the bulk of the alloy (mol/cm^3), C_s the hydrogen concentration in the surface of the alloy particles (mol/cm^3), d the density of the hydrogen storage alloy (g/cm^3) and t the discharge time (s). Thus, from the slope of a plot of $\log i$ versus t, according to Eq. (3), D/a^2 can be obtained, and D can be estimated if the radius of the particle a is known. From the slope of the linear portion of the corresponding plot in Fig. 10, the ratio of D/a^2 value is estimated by using Eq. (3) and listed in Table 3. It can be seen that the value of D/a^2 decreases drastically when La content in the alloys increases to 2.1 and over. Assuming all the $La_xMg_{3-x}Ni_9$ ($x = 1.6$–2.2) alloys have a similar particle distribution with the average particle radius of 13 μm, the hydrogen diffusion coefficient D of the alloy electrodes is calculated and listed in Table 3. It can be seen that the D of these alloy electrodes trends to decrease with increasing La content in the alloys rather mildly in the first region ($x = 2.0$), which agrees with the increased hydride stability of the La-rich alloys. The D value of the alloys with $x = 1.6$–2.0 shows a small change of (7.10–9.03) $\times$ 10^{-10} cm^2 s^{-1}, indicating that their HRD is controlled by the electrocatalytic activity for charge-transfer reaction. For the alloys with $x > 2.0$, the D value drops sharply to nearly only one-third of that of the alloys with $x \leq 2.0$. It is believed that the low hydrogen diffusion rate in these alloy electrodes become the cause for their poor high-rate dischargeability.

3.5. Cycle stability

Fig. 9 shows the discharge capacity of the alloy electrode as a function of cycle number. The cycling capacity retention rate, expressed as $S_{100}(\%) = C_{100}/C_{max} \times 100$ (where C_{max} is the maximum discharge capacity, C_{100} is the discharge capacity at the 100th cycles), after 100 cycles at 100 mA/g is also listed in Table 2. It is found that the capacity retention rate (S_{100}) of the alloy electrodes with composition ranged from $x = 1.6$ to 2.1 remains almost constant ($S_{100} = 60.4$–63.6%), while the S_{100} of the alloy electrode of $x = 2.2$ drops to 55.7%. It is well known that the cycling capacity decay of the hydrogen storage electrode is influenced mainly by two factors: the surface passivation due to the oxidation of active components to form oxides or hydroxides and the molar volume of hydrogen, V_H, in the hydride phase [7]. From the XRD analysis performed for the alloy electrode before and after 50 charge–discharge cycles (see Fig. 10), it is found that the $PuNi_3$-type structure of the

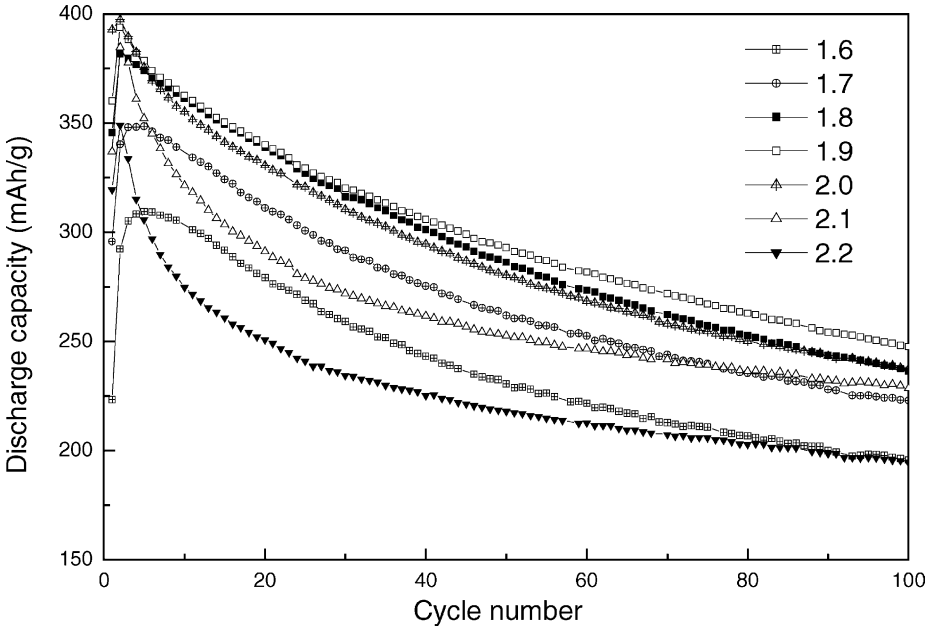

Fig. 9. Cycling stability of $La_xMg_{3-x}Ni_9$ ($x = 1.6$–2.2) alloys electrodes (discharge at 100 mA/g).

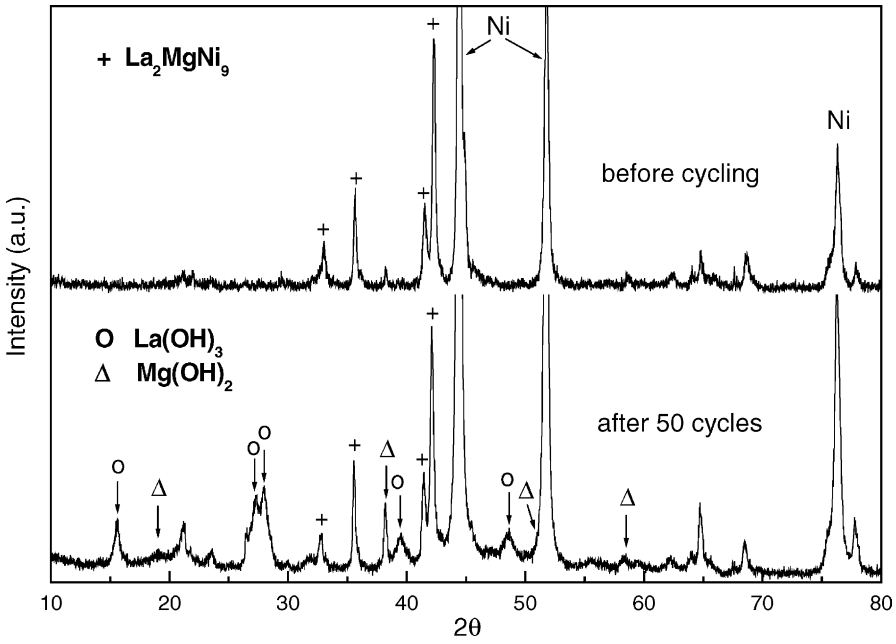

Fig. 10. The XRD patterns of La_2MgNi_9 alloy electrode before cycling and after 50 cycles (the peaks of Ni are from the carbonyl nickel powder in pressed alloy electrode).

alloy is preserved during the charge–discharge cycling process, and the diffraction peaks of $La(OH)_3$ and $Mg(OH)_2$ are clearly shown after cycling, as La and Mg on the surface of the alloy particles are oxidized to $La(OH)_3$ and $Mg(OH)_2$, respectively. As reported previously [22,23], the formation of passive layers of $La(OH)_3$ and $Mg(OH)_2$ on the alloy surface is ascribed as the main cause of cycling capacity degradation, because such a layer not only weakens the surface electrocatalytic activity and prevents the diffusion of hydrogen into/or from the alloy bulk, but also decreases the content of hydrogen absorption elements La and Mg in the alloys and thus reduces hydrogen storage capacity of the alloy. In addition, the corrosion rate of the active components during cycling is accelerated due to the large unit cell expansion rate ($\Delta V/V$) or the large V_H of the alloy hydrides as shown in Table 2, as the MH electrodes with a higher V_H undergoes a larger cell volume expansion and contraction during each charge and discharge cycle and a higher degree of alloy decrepitation upon cycling. This in turn leads to the increasing of the rate of contact of the fresh alloy surface with electrolyte and, consequently, a higher rate of corrosion and a larger capacity decay [7]. In spite of the improved electrochemical capacity of La–Mg–Ni system ternary alloy electrodes, their cycling stability is rather poor, and hence has to be upgraded for practical applications.

4. Conclusions

The effect of La/Mg ratio on the structure and electrochemical properties of the $La_xMg_{3-x}Ni_9$ ($x = 1.6$–2.2) alloys has been studied. It is found that all alloys are consisted of a main phase with hexagonal $PuNi_3$-type structure and a few impurity phases including $LaNi_5$ and $MgNi_2$. Both the unit cell volume and the hydride stability of the alloys increase with the increase in La/Mg ratio, but the discharge capacity of the alloys shows a maximum of 397.5 mAh/g at $x = 2.0$. The HRD_{1200} decrease with the increase of La/Mg ratio. The slower decrease of HRD_{1200} of the alloys with $x \leq 2.0$ is mainly attributed to the decrease of electrocatalytic activity of the alloys of the charge-transfer reaction, and the more rapid decrease of the alloys with $x > 2.0$ is mainly attributed to the lower hydrogen diffusion rate in the bulk of alloy. The cycling stability of La–Mg–Ni system ternary alloys is rather poor, as La and Mg are both corroded easily in KOH electrolyte and the large V_H of the hydride phase.

Acknowledgements

This work is supported by the National Nature Science Foundation of China (No. 50131040).

References

[1] T. Sakai, I. Uehara, H. Iwakura, J. Alloys Compd. 293–395 (1999) 762.
[2] S.R. Ovshinsky, M.A. Feteenko, J. Ross, Science 260 (1993) 176.
[3] D.M. Kim, K.J. Jang, J.Y. Lee, J. Alloys Compd. 293–395 (1999) 762.
[4] Y.Q. Lei, Y.M. Wu, Q.M. Yang, J. Wu, Q.D. Wang, Z. Phys. Chem. 183 (1994) 379.
[5] C. Iwakura, H. Inoue, S.G. Zhang, S. Nohaza, J. Alloys Compd. 270 (1998) 142.

[6] M. Tsukahara, K. Takahashi, T. Mishima, T. Sakai, H. Miyamura, N. Kuriyama, I. Uehara, J. Alloys Compd. 224 (1995) 162.
[7] J.J. Reilly, Metal hydrides electrodes, in: J.O. Besenhard (Ed.), Handbook of Battery Materials, Wiley, New York, 2000.
[8] K. Kadir, T. Sakai, I. Uahara, J. Alloys Compd. 257 (1997) 115.
[9] K. Kadir, N. Nuriyama, T. Sakai, I. Uehara, L. Eriksson, J. Alloys Compd. 284 (1999) 145.
[10] K. Kadir, T. Sakai, I. Uahara, J. Alloys Compd. 287 (1999) 264.
[11] K. Kadir, T. Sakai, I. Uahara, J. Alloys Compd. 302 (2000) 112.
[12] J. Chen, H.T. Takeshita, H. Tanaka, N. Kuriyama, T. Sakai, J. Alloys Compd. 302 (2000) 304.
[13] J. Chen, N. Kuriyama, H.T. Takeshita, H. Tanaka, T. Sakai, M. Haruta, Electrochem. Solid-State Lett. 3 (6) (2000) 249.
[14] T. Kohno, H. Yoshida, F. Kawashima, T. Inaba, I. Sakai, M. Yamamoto, M. Kanda, J. Alloys Compd. 311 (2000) L5.
[15] H.G. Pan, Y.F. Liu, M.X. Gao, Y.Q. Lei, Q.D. Wang, J. Electrochem. Soc. 150 (5) (2003) A565.
[16] B. Liao, Y.Q. Lei, G.L. Lu, L.X. Chen, H.G. Pan, Q.D. Wang, J. Alloys Compd. 356–357 (2003) 746.
[17] W. Weppner, R.A. Huggins, J. Electrochem. Soc., Solid State Sci. Technol. 1569 (1977).
[18] P.H.L. Notten, P. Hokkeling, J. Electrochem. Soc. 138 (1991) 1877.
[19] C. Iwakura, T. Oura, H. Inoue, M. Matsuoka, Electrochem. Acta 41 (1) (1996) 117.
[20] C. Iwakura, M. Matsuoka, K. Asai, T. Kohno, J. Power Source 38 (1992) 335.
[21] G. Zheng, B.N. Popov, R.E. White, J. Electrochem. Soc. 142 (1995) 2695.
[22] D.L. Sun, Y.Q. Lei, W.H. Liu, J.J. Jiang, J. Wu, Q.D. Wang, J. Alloys Compd. 231 (1995) 621.
[23] J.J. Willems, Philips J. Res. 39 (Suppl. 1) (1984) 1.